Enhancement of the anomalous Nernst effect in Ni/Pt superlattices

T. Seki, 1,2,3,* Y. Sakuraba, 3,4 K. Masuda, 3 A. Miura, 3 M. Tsujikawa, 2,5 K. Uchida, 1,2,3 T. Kubota, 1,2 Y. Miura, 3 M. Shirai, 2,5,6 and K. Takanashi, 2,6

1 Institute for Materials Research, Tohoku University, Sendai 980-8577, Japan

2 Center for Spintronics Research Network, Tohoku University, Sendai 980-8577, Japan

3 National Institute for Materials Science, Tsukuba 305-0047, Japan

4 PRESTO, Japan Science and Technology Agency, Saitama 322-0012, Japan

5 Research Institute of Electrical Communication, Tohoku University, Sendai 980-8577, Japan

6 Center for Science and Innovation in Spintronics, Core Research Cluster, Tohoku University, Sendai 980-8577, Japan



(Received 15 September 2020; revised 15 November 2020; accepted 15 December 2020; published 6 January 2021)

We report an enhancement of the anomalous Nernst effect (ANE) in Ni/Pt (001) epitaxial superlattices. The transport and magnetothermoelectric properties were investigated for the Ni/Pt superlattices with various Ni layer thicknesses (t). The anomalous Nernst coefficient was increased up to more than $1 \mu V K^{-1}$ for $2.0 \text{ nm} \le t \le 4.0 \text{ nm}$, which was the remarkable enhancement compared to the bulk Ni. It has been found that the large transverse thermoelectric conductivity (α_{xy}), reaching $\alpha_{xy} = 4.8 \text{ A K}^{-1} \text{ m}^{-1}$ for t = 4.0 nm, plays a prime role for the enhanced ANE of the Ni/Pt (001) superlattices.

DOI: 10.1103/PhysRevB.103.L020402

Spin caloritronics [1], the field studying the interconversion between charge current (\mathbf{J}_c) and heat current (\mathbf{J}_q) mediated by spin current (\mathbf{J}_s) and/or magnetization (\mathbf{M}) , has attracted attention not only for academic interests but also for practical applications. The spin caloritronic phenomena such as spin Seebeck effect [2-4] have stimulated the renewed interest in the well-known thermoelectric phenomena in ferromagnets. One of the thermoelectric phenomena in ferromagnets is the anomalous Nernst effect (ANE), in which J_c appears in the cross-product direction of M and a temperature gradient (∇T) . Although ANE has been known for a long time, the microscopic physical picture for ANE has not fully been understood. In addition to the fundamental point of view, this magnetothermoelectric effect is possibly beneficial for thermoelectric conversion applications [5,6]. The key for the ANE-based thermoelectric conversion is to find a material with a large anomalous Nernst coefficient (S^{ANE}) because the charge current density induced by ANE ($\mathbf{j}_{c,ANE}$) is given by $\mathbf{j}_{c,ANE} = \sigma S^{ANE} \{ (\mathbf{M}/|\mathbf{M}|) \times \nabla T \}$ with electrical conductivity (σ) [7].

Several ferromagnets show the ANE and the anomalous Ettingshausen effect as the reciprocal phenomenon [8–16]. We previously reported the enhancement of ANE in the metallic multilayers of Fe/Pt, Fe/Au, and Fe/Cu [17]. The increased ANE with the number of interfaces was reported for the Co/Pt superlattices [18]. These studies imply the low dimensionality of layer and/or the existence of interface plays a crucial role for the increase in ANE, and one may be aware that metallic multilayers or superlattices with a number of interfaces are promising for achieving a large ANE.

Among several choices for a ferromagnet and a paramagnet consisting of the metallic superlattice, this study focuses on ferromagnetic Ni and paramagnetic Pt. Ni is a material exhibiting the large anisotropic magneto-Peltier effect thanks to its characteristic electronic structure [19,20] and is an interesting material from the viewpoint of ANE [21]. Pt is a representative paramagnet having the large spinorbit interaction. This large spin-orbit interaction of Pt is probably advantageous for the ANE of Ni through the interface. Recently, we prepared the perpendicularly magnetized Ni/Pt (001) epitaxial superlattices directly on a nonconductive SrTiO₃ substrate [22]. The Ni/Pt (001) epitaxial superlattices are suitable for studying the effects of layer thickness and interface on the magnitude of ANE, and available to compare the experiment with theoretical calculation. This Letter reports the investigation of ANE in the Ni/Pt (001) epitaxial superlattices with various Ni layer thicknesses (t). In addition to the evaluation of S^{ANE} , the value of S^{ANE} divided by saturation magnetization (M_s) is shown, which is an indicator for the ANE-based thermopiles integrated densely [23]. We found the enhanced ANE of the Ni/Pt (001) superlattices, which is attributable to the large transverse thermoelectric conductivity (α_{xy}).

 $[\mathrm{Ni}(t)/\mathrm{Pt}(1.0~\mathrm{nm})]_{\times N}$ superlattices were grown on SrTiO₃ (100) single crystal substrates employing magnetron sputtering with the base pressure below $2\times10^{-7}~\mathrm{Pa}$. The deposition temperature was set at 400 °C for the Ni and Pt layers. The Ni layer was first deposited, which was followed by the layers of $[\mathrm{Pt/Ni}]_{\times N-1}/\mathrm{Pt}$. Finally, a 2-nm-thick Al layer was deposited at room temperature as a capping layer. The substrate temperature of 400 °C was necessary to achieve the (001) epitaxial growth, and the well-defined layered structures were achieved without remarkable intermixing between the layers [22]. The magnetic properties were measured using a vibrating sample

^{*}go-sai@imr.tohoku.ac.jp

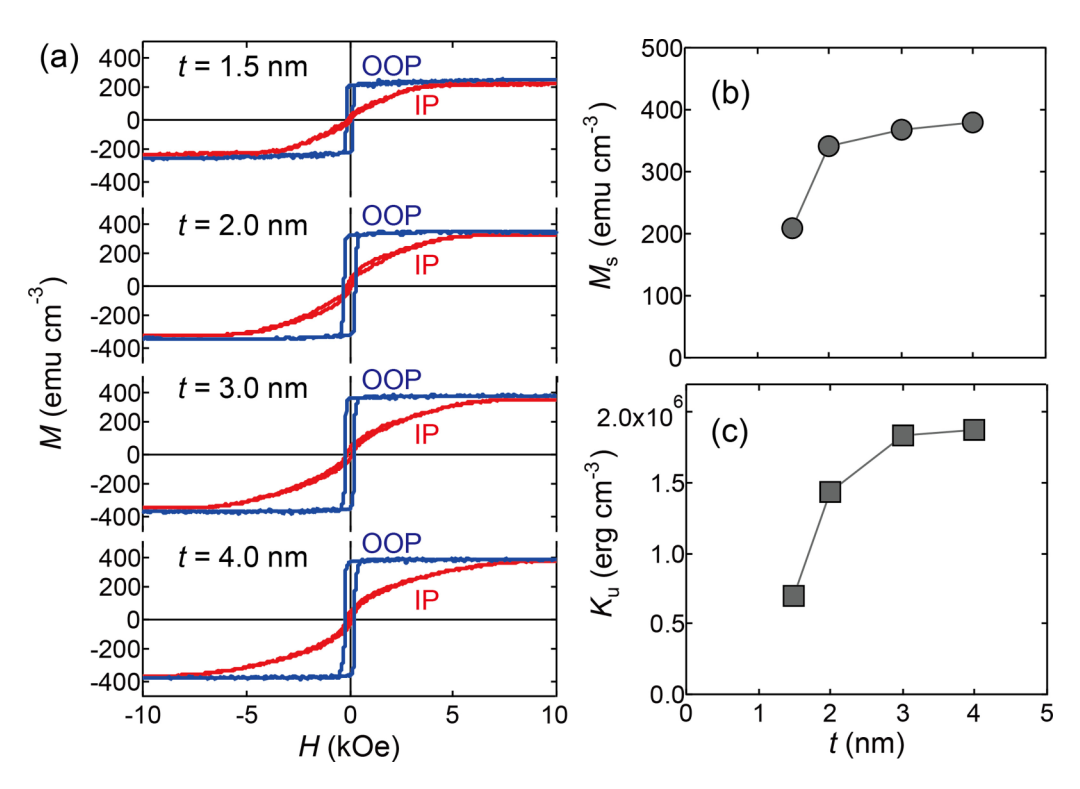


FIG. 1. (a) Magnetization curves for the $[\mathrm{Ni}(t)/\mathrm{Pt}(1.0~\mathrm{nm})]_{\times N}$ with t=1.5, 2.0, 3.0, and 4.0 nm, where N was set to be 8, 7, 5, and 4, respectively. The red curves denote the magnetization curves measured with the magnetic field (H) applied in the film plane (IP curve) while the blue curves denote those measured with out-of-plane magnetic field (OOP curve). (b) Saturation magnetization (H_0) and (c) uniaxial magnetic anisotropy constant (H_0) as a function of H_0 .

magnetometer (VSM) at room temperature. The Hall-cross shapes were patterned employing photolithography and Ar ion milling. This study exploited two different Hall-cross-shaped devices in accordance with the purpose of measurement: one is for the electrical transport measurement, and the other is for the thermoelectric measurement. For the electrical transport measurement, the devices were installed into the physical properties measurement system (PPMS, Quantum Design, Inc.), and the magnetic field dependence of longitudinal (ρ_{xx}) and transverse resistivities (ρ_{xy}) was measured at various temperature (T). For evaluating ANE, we gave ∇T to the in-plane direction and applied external magnetic field to the perpendicular direction to the device to measure the electric field (E_{ANE}) arising from ANE in PPMS. ∇T in PPMS was carefully estimated using the procedure described in Refs. [13–15] with the infrared camera. The Seebeck effects as well as σ for the blanket films were measured employing the Seebeck coefficient/electric resistance measurement system (ZEM-3, ADVANCE RIKO, Inc.). All the thermoelectric properties were measured at room temperature.

Figure 1(a) shows the magnetization curves for the $[Ni/Pt]_{\times N}$ with t=1.5, 2.0, 3.0, and 4.0 nm, where N was set to be 8, 7, 5, and 4, respectively. Those repetition numbers were adjusted for the total thicknesses of approximately 20 nm. The red curves denote the magnetization curves measured with the magnetic field (H) applied in the film plane (IP curve) while the blue curves denote those measured with the out-of-plane H (OOP curve). In this study, M was defined as the detected magnetic moment per the unit volume of Ni layers. All the films show the perpendicular magnetization.

The effective uniaxial magnetic anisotropy constant ($K_{\rm eff}$) corresponds to the area enclosed between the OOP and IP curves. The values of $M_{\rm s}$ and uniaxial magnetic anisotropy constant ($K_{\rm u}$) as a function of t are plotted in Figs. 1(b) and 1(c), where $K_{\rm u} = K_{\rm eff} + 2\pi M_{\rm s}^2$. $M_{\rm s}$ is decreased as t is reduced, which results from the decrease in Curie temperature at the small t [22]. $K_{\rm u}$ also shows the reduction with decreasing t. This t dependence of $K_{\rm u}$ is partially related with that of $M_{\rm s}$. The other reason is that the adequate thickness region to obtain the large $K_{\rm u}$ exists for the Ni / Pt (001) superlattice, which is $2.0 \, {\rm nm} \leqslant t \leqslant 4.0 \, {\rm nm}$ as reported previously [22].

The electrical transport properties were measured as illustrated in Fig. 2(a), where the width of the Hall bar is 10 μ m and the edge-to-edge distance between the Hall branches is 50 μ m. The longitudinal (V_{xx}) and transverse voltage (V_{xy}) were measured under the dc current (I_{dc}) application and perpendicular $H(H_z)$. Figure 2(a) displays the transverse resistance (R_{xy}) for the device with t = 3.0 nm. The square-shaped hysteresis is observed. ρ_{xy} is composed of two terms: ordinary Hall effect and anomalous Hall effect (AHE). For the present perpendicularly magnetized sample, ρ_{xy} at $H_z = 0$ Oe is the value coming from only the AHE term. Figures 2(b) and 2(c) plot the longitudinal conductivity (σ_{xx}) and the transverse conductivity (σ_{xy}) , respectively, at $H_z = 0$ Oe as a function of T. Regardless of t, the metallic behavior is observed in the T dependence of conductivities. Figure 2(d) corresponds to the σ_{xx} versus $|\sigma_{xy}|$ plot. Onoda et al. [24] mentioned that σ_{xy} shows a gradual dependence on σ_{xx} and becomes constant of $10^2 - 10^3 \,\Omega^{-1} \,\mathrm{cm}^{-1}$ in the moderately dirty region of $3 \times 10^3 \,\Omega^{-1} \,\mathrm{cm}^{-1} \leqslant \sigma_{xx} \leqslant 5 \times 10^5 \,\Omega^{-1} \,\mathrm{cm}^{-1}$. Although

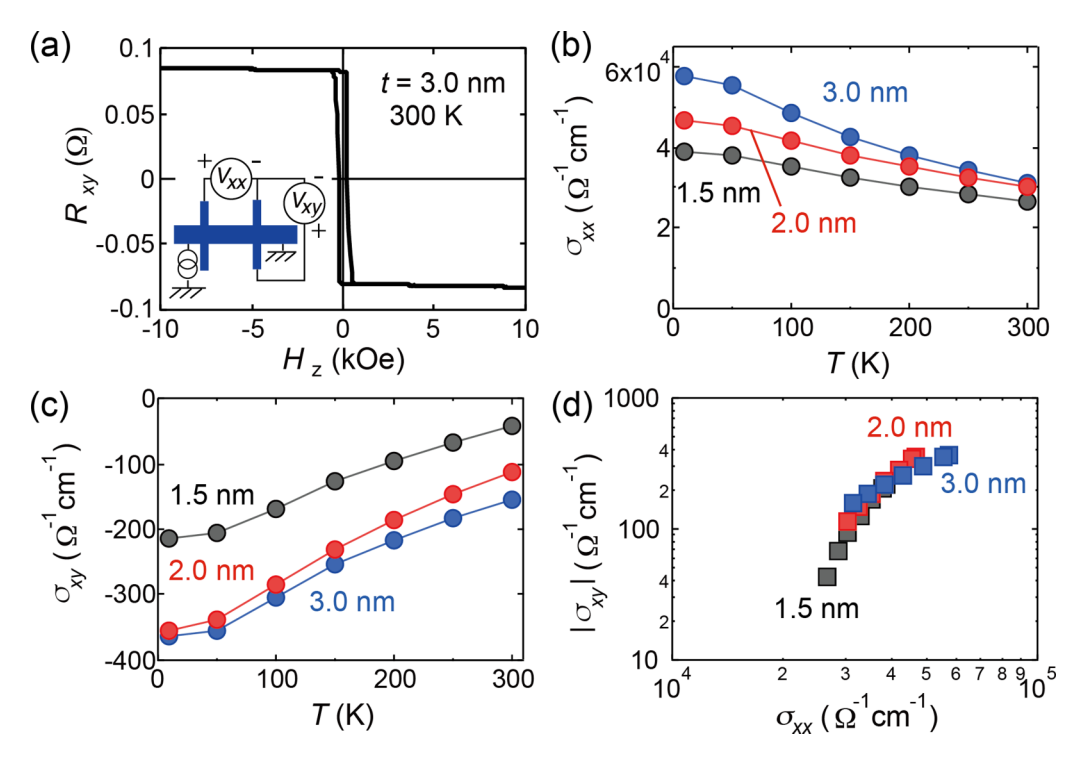


FIG. 2. (a) Transverse resistance (R_{xy}) as a function of perpendicular magnetic field (H_z) for the device with t=3.0 nm. Inset: the illustration of Hall device structure and measurement setup. (b) Longitudinal conductivity (σ_{xx}) and (c) transverse conductivity (σ_{xy}) , at $H_z=0$ Oe as a function of measurement temperature (T). (d) σ_{xx} vs $|\sigma_{xy}|$ plot.

the present result roughly follows the theoretical tendency [24], suggesting that the intrinsic mechanism is dominant, σ_{xy} shows a positive correlation with σ_{xx} rather than the constant against σ_{xx} . The reason for this scaling is not clear at present.

Figure 3(a) depicts the measurement setup for the ANE. By heating one side of the substrate, ∇T was induced along the in-plane x direction. H was applied along the out-ofplane z direction. As a result, the E_{ANE} was detected along the y direction. The values of S^{ANE} were measured for the Hall-cross-shaped devices with 2.0-mm-wide channel and 2.1-mm-wide branches. Before microfabricating the devices, the Seebeck coefficient (S) and the longitudinal conductivities were measured for the blanket films. We also evaluated the AHE using the Hall-cross-shaped devices that were used for ANE measurement. In this study, when those parameters were obtained, the whole multilayer was regarded as one ferromagnetic material. Figure 3(b) shows the H dependence of $E_{\rm ANE}$ divided by ∇T for $t = 3.0 \, \text{nm}$. The square-shaped hysteresis of $E_{\text{ANE}}/\nabla T$, which resembles the magnetization curve [Fig. 1(a)], was definitely observed. S^{ANE} was calculated from the slope of linear fit to E_{ANE} as a function of ∇T [inset of

Figure 3(c) plots the t dependence of S^{ANE} . All the samples exhibit the large values of $S^{\text{ANE}} \geqslant 0.9 \,\mu\text{V K}^{-1}$, and the maximum $S^{\text{ANE}} = 1.14 \pm 0.05 \,\mu\text{V K}^{-1}$ was obtained at $t = 2.0 \,\text{nm}$. It is noted that these S^{ANE} for the present Ni/Pt superlattices are one order of magnitude of larger than that for the bulk Ni [12,25]. In order to elucidate the enhanced ANE for the Ni/Pt superlattice, S and ρ_{xy}/ρ_{xx} referred to the AHE angle are plotted as a function of t in Figs. 3(d) and 3(e), respectively, where $\rho_{xy} = -\sigma_{xy}/\sigma_{xx}^2$. Although the sign change of S cannot be clearly explained, it may come from the

Ni-Pt alloy [25] formed at the interface. Using the resistivity tensor, S^{ANE} is expressed as [15]

$$S^{\text{ANE}} = \rho_{\text{rr}} \alpha_{\text{rv}} + \rho_{\text{rv}} \alpha_{\text{rr}}, \tag{1}$$

where α_{xx} is given by S/ρ_{xx} . The second term of Eq. (1) comes from the Seebeck effect-induced charge current, i.e., $S\rho_{xy}/\rho_{xx}$. On the other hand, the first term of Eq. (1) expresses the contribution of direct generation of transverse charge current originating from α_{xy} . Figure 3(f) shows the t dependence of $\rho_{xy}\alpha_{xx}$, which is two orders of magnitude smaller than S^{ANE}. This fact definitely indicates that the conversion process through the Seebeck effect followed by AHE hardly contributes to the ANE of the Ni/Pt superlattices. Since the AHE angle of Ni/Pt superlattices is not so small compared to other ferromagnets [25], the small S is the reason for the small $\rho_{xy}\alpha_{xx}$ In contrast to α_{xx} , α_{xy} is the essential parameter of the large ANE of the Ni/Pt superlattices. The values of α_{xv} have been estimated using the obtained parameters of S^{ANE} , ρ_{xx} , ρ_{xy} , and S. Figures 3(g) and 3(h) show α_{xy} and ρ_{xx} , respectively. The Ni/Pt superlattices possess very large α_{xy} , and the maximum value is $\alpha_{xy} = 4.8 \,\mathrm{A \, K^{-1} \, m^{-1}}$ at $t = 4.0 \,\mathrm{nm}$. This α_{xy} is comparable to or larger than several materials exhibiting large ANE such as Co₂MnGa $(2.4-3.0 \,\mathrm{A\,K^{-1}\,m^{-1}})$ [9], $\mathrm{Co_3Sn_2S_2}$ ($\sim 2\,\mathrm{A\,K^{-1}\,m^{-1}}$) [26], and $SmCo_5$ (4.6 A K^{-1} m⁻¹) [12]. All the experimental data are summarized in the Supplemental Material [27] (see also Refs. [21,28–32]).

In addition to the finding of large α_{xy} , another feature of Ni/Pt superlattice is the large value of $S^{\rm ANE}$ per magnetization, i.e., $S^{\rm ANE}/M_{\rm s}$. As shown in Fig. 3(i), $S^{\rm ANE}/M_{\rm s}$ is remarkably increased for small t, e.g., $3.6~\mu{\rm V~K^{-1}~T^{-1}}$ at t=1.5 nm. The sample with t=1.5 nm showing the small $M_{\rm s}$ still maintains

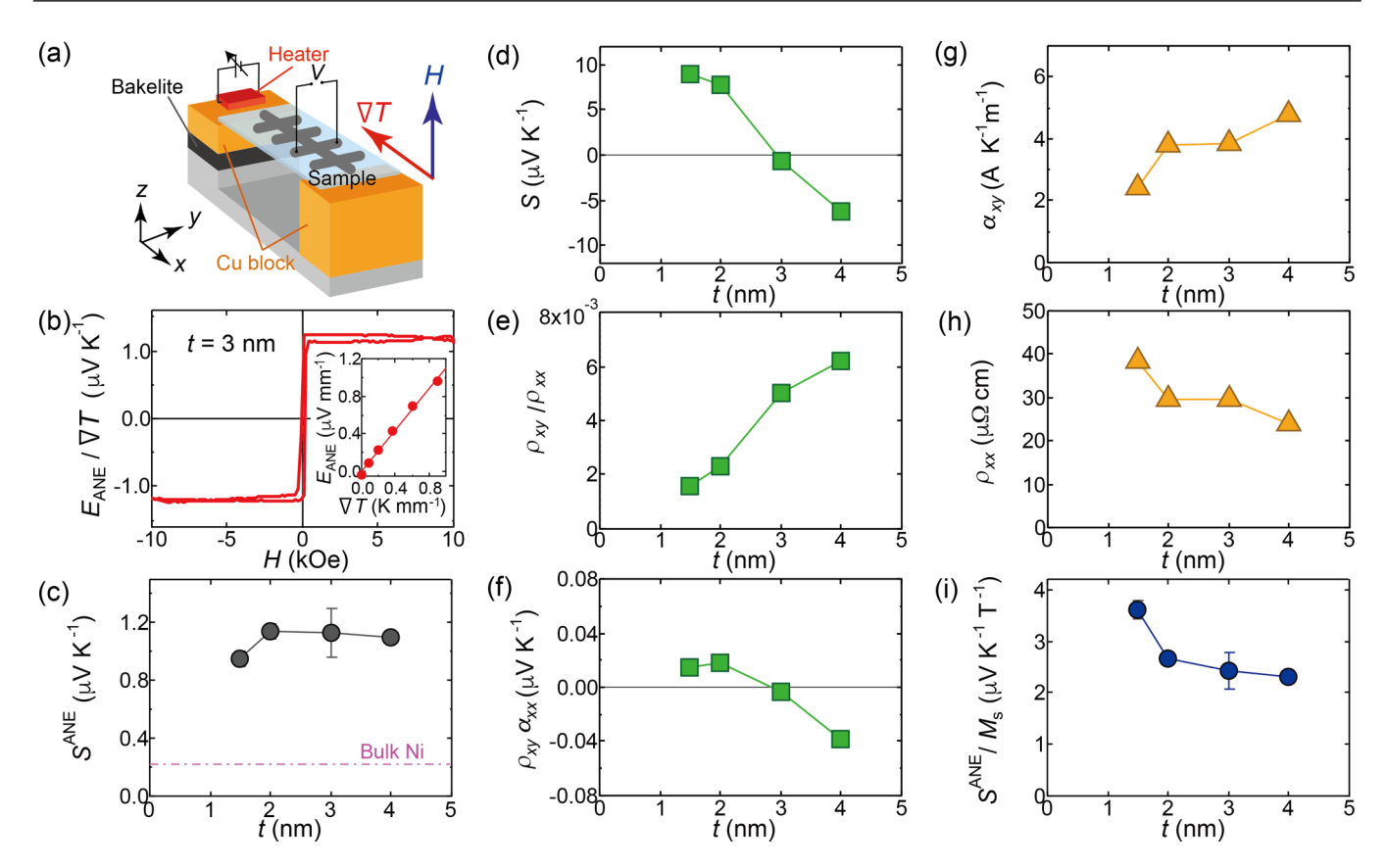


FIG. 3. (a) Measurement setup for anomalous Nernst effect (ANE). (b) H dependence of electric field induced by ANE (E_{ANE}) divided by ∇T for the device with t=3.0 nm. Inset: the plot of E_{ANE} as a function of ∇T . (c) t dependence of anomalous Nernst coefficient (S^{ANE}), (d) Seebeck coefficient (S^{ANE}), (e) ρ_{xy}/ρ_{xx} , (f) $\rho_{xy}\alpha_{xx}$, (g) transverse Peltier coefficient (α_{xy}), (h) ρ_{xx} , and (i) S^{ANE}/M_s . In (c), the dashed-dotted line denotes the value for the bulk Ni reported in Ref. [12].

large $S^{\rm ANE}$. This interestingly means that the value of $S^{\rm ANE}$ is not proportional to the magnitude of $M_{\rm s}$ even for the identical superlattices. The present Ni/Pt superlattices do not follow the relationship between $S^{\rm ANE}$ and $M_{\rm s}$ mentioned in Ref. [23]. For practical applications, this large $S^{\rm ANE}$ and small $M_{\rm s}$ could be promising to improve the thermoelectric conversion performance as discussed in Refs. [14,23,33].

One may consider the following contributions for explaining the enhanced ANE: (i) alloying of Ni and Pt at the interfaces, (ii) proximity-induced magnetic moments in Pt [34,35], and (iii) spin-orbit interaction at the interfaces. All these possibilities originate from the interface. Since the decrease in t at the fixed total thickness (t_{total}) means the increase in the interface density, S^{ANE} should increase with reducing t if these interface effects are dominant. However, S^{ANE} does not increase remarkably at the small t. Thus, we need to consider another possible contribution. For this purpose, the first-principles calculations were made for σ_{xy} and σ_{xy} . As described above, the large σ_{xy} leads to the enhanced ANE. σ_{xy} is expressed as [36]

$$\alpha_{xy} = -\frac{\pi^2}{3} \frac{k_{\rm B}^2 T}{e} \left(\frac{\partial \sigma_{xy}}{\partial \varepsilon} \right)_{E_{\rm E}},\tag{2}$$

where $k_{\rm B}$ is the Boltzmann constant and e is the elementary charge of electron. $(\partial \sigma_{xy}/\partial \varepsilon)_{E_{\rm F}}$ is the energy derivative of σ_{xy} at the Fermi level $(E_{\rm F})$. The density-functional theory (DFT) with the aid of the Vienna ab initio simulation program (VASP)

was used for the calculations [28]. For details, see the Supplemental Material [27]. The generalized gradient approximation (GGA) was adopted for the exchange-correlation energy [29], and the projector augmented wave pseudopotential [30,31] was used to treat the core electrons properly. In this study, we examined the effect of formation of periodic structure on σ_{xy} and α_{xy} by inserting the Pt layer into the Ni. Figure 4 shows the σ_{xy} and α_{xy} versus chemical potential (μ) for the Ni 14 monolayer (ML)/Pt d_{Pt} ML (Ni14/Pt d_{Pt}), where d_{Pt} was set at 0, 2, 4, and 6, the Ni 14 ML with the vacuum interface (Ni14/vac), and the bulk Ni. Here, $\mu = 0$ corresponds to $E_{\rm F}$. The in-plane lattice constants were set to 0.372 nm for the Ni 14 ML, which was determined from the experimental value [22], and 0.352 nm for the bulk Ni. For the present calculation, the Coulomb interaction (U) of 3.9 eV and the Hund coupling (J) of 1.1 eV are considered in Ni 3d states as well as [21]. As shown in Fig. 4(a), the bulk Ni and Ni14/Pt0 exhibit similar μ dependence. Note here that Ni14Pt0 does not include the vacuum layer, and a small difference between the bulk Ni and Ni14/Pt0 comes from the difference in the in-plane lattice constants. However, a drastic change is observed for Ni14/vac [Fig. 4(a)] and Ni14/Pt d_{Pt} with $d_{Pt} = 2$, 4, and 6 [Fig. 4(b)]. Fine oscillatory behavior is seen in σ_{xy} versus μ . Because this feature is not observed for bulk Ni, the oscillation is attributable to the formation of interface. This oscillation in σ_{xy} against μ leads to the increase in energy derivative of σ_{xy} . Let us here remember that the large derivative of σ_{xy}

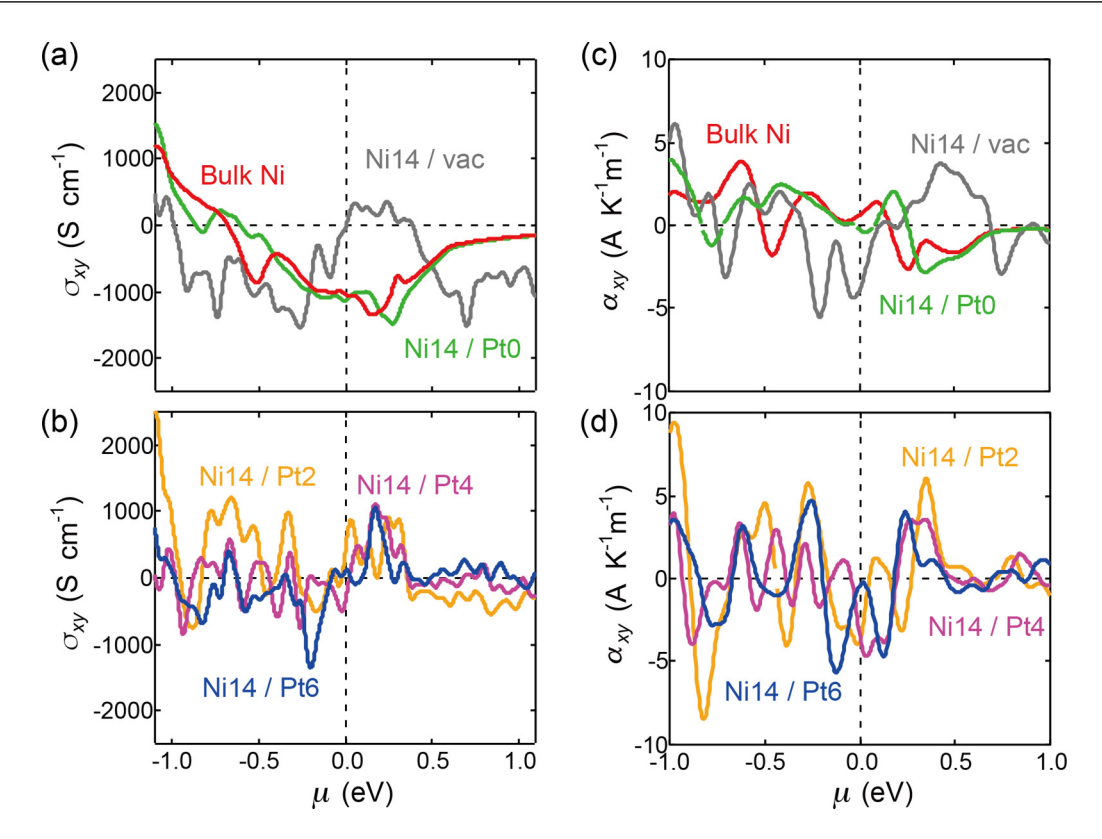


FIG. 4. First-principles calculation of σ_{xy} (a), (b) and α_{xy} (c), (d) vs chemical potential (μ) for the Ni 14 monolayer (ML)/Pt d_{Pt} ML, where d_{Pt} was set at 0, 2, 4, and 6, the Ni 14 ML with the vacuum interface, and the bulk Ni. The calculations for α_{xy} were carried out at 300 K.

yields a large α_{xy} following Eq. (2). As a result, the larger $|\alpha_{xy}|$ than that of bulk Ni was obtained at many μ values for Ni14/vac [Fig. 4(c)] and Ni14/Pt d_{Pt} with $d_{Pt} = 2$, 4, and 6 [Fig. 4(d)]. The band structures and the Berry curvatures were calculated in Ni14/Pt6 and Ni14/Pt0 (see Supplemental Material Fig. 1 [27]). The band-folding effect provides many band dispersions around $E_{\rm F}$ in the $(k_{\rm r}, k_{\rm v})$ plane (corresponding to in-plane wave vectors) and the hybridizations of these bands lead to many band splittings. This is the origin for the oscillation in the Berry curvature, and the resultant oscillatory behavior of σ_{xy} . From these results, we may say that the oscillatory behavior in σ_{xy} due to the interface formation is related with the enhanced ANE. In addition to the calculation for various d_{Pt} , the cases with various Ni ML (d_{Ni}) were calculated as shown in the Supplemental Material [27] and all the cases show the similar oscillation in σ_{xy} . Although this interface formation is another possible scenario, the present calculation cannot fully explain the t dependence of S^{ANE} because the amplitude and energy position of oscillation in σ_{xy} do not simply vary with d_{Pt} or d_{Ni} . For quantitative comparison and more concrete examination, further systematic studies with other materials systems including the effects of structural imperfections and/or phonon/magnon excitations are required.

Hereafter, let us discuss the contribution of interface with the SrTiO₃ substrate. The high-density two-dimensional electron gas confined at the interface with SrTiO₃ is famous for its large Seebeck coefficient [37]. If an oxygen-deficient layer and/or a Ni-doped layer exist at the interface and becomes conductive, they may affect the ANE signals. For investigating

the influence of the SrTiO₃ substrate, we also prepared the $[Ni(3.0 \text{ nm})/Pt(1.0 \text{ nm})]_{\times N}$ superlattices with different repetition numbers: N=3, 5, 10, and 20. The different N leads to the different t_{total} of Ni/Pt superlattice. Table I summarizes S^{ANE} for the samples with different N (t_{total}). There is no remarkable difference in S^{ANE} between N=5, N=10, and N=20. However, a definite increase in S^{ANE} is seen for N=3, suggesting the possibility that the ANE signal originating from the interface with the SrTiO₃ substrate is included in the S^{ANE} for small N. Judging from this, we consider that the contribution from the SrTiO₃ substrate is negligibly small at $t_{\text{total}} \geqslant 20 \text{ nm}$.

Finally, we quantitatively compare $S^{\rm ANE}$ for the Ni/Pt superlattices to those for bulk Ni and a Ni single layer film. According to Ref. [12], the bulk Ni showed $S^{\rm ANE} = 0.22~\mu{\rm V~K^{-1}}$. As a reference sample, we also prepared a 20-nm-thick Ni single layer on a SrTiO₃ substrate, which showed $S^{\rm ANE} = 0.52 \pm 0.05~\mu{\rm V~K^{-1}}$. Those values are smaller than the maximum $S^{\rm ANE}$ for the Ni/Pt superlattices. One may think that the large transverse Peltier coefficient (2.4 A K⁻¹ m⁻¹ \leq

TABLE I. Anomalous Nernst coefficient (S^{ANE}) for $[\text{Ni}(3.0 \text{ nm})/\text{Pt}(1.0 \text{ nm})]_{\times N}$ superlattices with different repetitions.

	N = 3	N = 5	N = 10	N = 20
t_{total} (nm)	12.0	20.0	40.0	80.0
$S^{\text{ANE}} (\mu V K^{-1})$	1.49 ± 0.17	1.13 ± 0.17	1.14 ± 0.18	1.17 ± 0.05

 $\alpha_{xy} \leq 4.8 \,\mathrm{A \, K^{-1} \, m^{-1}}$) is the key parameter for enhancing ANE in Ni/Pt superlattices. Although α_{xy} for bulk Ni is as large as $2.6 \,\mathrm{A \, K^{-1} \, m^{-1}}$ [25] and is comparable to that for $t=1.5 \,\mathrm{nm}$, the reduced α_{xy} may be related with the reduced M_{S} . The α_{xy} is definitely enhanced for the samples with thicker Ni layers. In addition, the small ρ_{xx} ($\sim 9 \,\mu\Omega$ cm) for bulk Ni give rise to S^{ANE} one order of magnitude smaller than that for the Ni/Pt superlattices. This fact suggests that the formation of superlattice allows us to control several key parameters independently thanks to the degrees of freedom in design that the superlattice structure possesses.

In summary, we demonstrated the enhancement of ANE owing to the formation of Ni/Pt superlattices. The value of $S^{\rm ANE}$ was increased up to more than $1~\mu \rm V~K^{-1}$ for the samples with $2.0~\rm nm \leqslant t \leqslant 4.0~\rm nm$, and the large $S^{\rm ANE}/M_{\rm s} = 3.6~\mu \rm V~K^{-1}~T^{-1}$ was achieved for $t=1.5~\rm nm$. The enhanced

ANE is attributable to the large α_{xy} . We believe that the present study provides a strategy to enhance ANE.

The authors thank K. Ito and H. Kurebayashi for their valuable comments and M. Isomura and B. Masaoka for technical support. The device fabrication was partly carried out at the Cooperative Research and Development Center for Advanced Materials, IMR, Tohoku University. This work was supported by the Grant-in-Aid for Scientific Research (S) (Grant No. JP18H05246) from JSPS KAKENHI, PRESTO from the Japan Science and Technology Agency (No. JPMJPR17R5), and CREST "Creation of Innovative Core Technologies for Nano-enabled Thermal Management" (Grant No. JPMJCR17I1) from JST, Japan. A.M. was supported by JSPS through a research fellowship for young scientists (Grant No. JP18J02115).

- [1] G. E. W. Bauer, E. Saitoh, and B. J. van Wees, Nat. Mater. 11, 391 (2012).
- [2] K. Uchida, S. Takahashi, K. Harii, J. Ieda, W. Koshibae, K. Ando, S. Maekawa, and E. Saitoh, Nature (London) 455, 778 (2008).
- [3] K. Uchida, J. Xiao, H. Adachi, J. Ohe, S. Takahashi, J. Ieda, T. Ota, Y. Kajiwara, H. Umezawa, H. Kawai, G. E. W. Bauer, S. Maekawa, and E. Saitoh, Nat. Mater. 9, 894 (2010).
- [4] C. M. Jaworski, J. Yang, S. Mack, D. D. Awschalom, J. P. Heremans, and R. C. Myers, Nat. Mater. 9, 898 (2010).
- [5] Y. Sakuraba, Scr. Mater. 111, 29 (2016).
- [6] Y. Sakuraba, K. Hasegawa, M. Mizuguchi, T. Kubota, S. Mizukami, T. Miyazaki, and K. Takanashi, Appl. Phys. Exp. 6, 033003 (2013).
- [7] T. Seki, R. Iguchi, K. Takanashi, and K. Uchida, J. Phys. D: Appl. Phys. 51, 254001 (2018).
- [8] K. Hasegawa, M. Mizuguchi, Y. Sakuraba, T. Kamada, T. Kojima, T. Kubota, S. Mizukami, T. Miyazaki, and K. Takanashi, Appl. Phys. Lett. 106, 252405 (2015).
- [9] A. Sakai, Y. P. Mizuta, A. A. Nugroho, R. Sihombing, T. Koretsune, M. Suzuki, N. Takemori, R. Ishii, D. Nishio-Hamane, R. Arita, P. Goswami, and S. Nakatsuji, Nat. Phys. 14, 1119 (2018).
- [10] T. Seki, R. Iguchi, K. Takanashi, and K. Uchida, Appl. Phys. Lett. 112, 152403 (2018).
- [11] H. Reichlova, R. Schlitz, S. Beckert, P. Swekis, A. Markou, Y. Chen, D. Kriegner, S. Fabretti, G. H. Park, A. Niemann, S. Sudheendra, A. Thomas, K. Nielsch, C. Felser, and S. T. B. Goennenwein, Appl. Phys. Lett. 113, 212405 (2018).
- [12] A. Miura, H. Sepehri-Amin, K. Masuda, H. Tsuchiura, Y. Miura, R. Iguchi, Y. Sakuraba, J. Shiomi, K. Hono, and K. Uchida, Appl. Phys. Lett. 115, 222403 (2019).
- [13] H. Nakayama, K. Masuda, J. Wang, A. Miura, K. Uchida, M. Murata, and Y. Sakuraba, Phys. Rev. Mater. 3, 114412 (2019).
- [14] W. Zhou and Y. Sakuraba, Appl. Phys. Exp. 13, 043001 (2020).
- [15] Y. Sakuraba, K. Hyodo, A. Sakuma, and S. Mitani, Phys. Rev. B 101, 134407 (2020).

- [16] A. Miura, K. Masuda, T. Hirai, R. Iguchi, T. Seki, Y. Miura, H. Tsuchiura, K. Takanashi, and K. Uchida, Appl. Phys. Lett. 117, 082408 (2020).
- [17] K. Uchida, T. Kikkawa, T. Seki, T. Oyake, J. Shiomi, Z. Qiu, K. Takanashi, and E. Saitoh, Phys. Rev. B 92, 094414 (2015).
- [18] C. Fang, C. H. Wan, Z. H. Yuan, L. Huang, X. Zhang, H. Wu, Q. T. Zhang, and X. F. Han, Phys. Rev. B 93, 054420 (2016).
- [19] K. Uchida, S. Daimon, R. Iguchi, and E. Saitoh, Nature (London) 558, 95 (2018).
- [20] K. Masuda, K. Uchida, R. Iguchi, and Y. Miura, Phys. Rev. B 99, 104406 (2019).
- [21] J. Weischenberg, F. Freimuth, S. Blügel, and Y. Mokrousov, Phys. Rev. B 87, 060406(R) (2013).
- [22] T. Seki, M. Tsujikawa, K. Ito, K. Uchida, H. Kurebayashi, M. Shirai, and K. Takanashi, Phys. Rev. Mater. 4, 064413 (2020).
- [23] M. Ikhlas, T. Tomita, T. Koretsune, M. Suzuki, D. Nishio-Hamane, R. Arita, Y. Otani, and S. Nakatsuji, Nat. Phys. 13, 1085 (2017).
- [24] S. Onoda, N. Sugimoto, and N. Nagaosa, Phys. Rev. B 77, 165103 (2008).
- [25] A. Miura, R. Iguchi, T. Seki, K. Takanashi, and K. Uchida, Phys. Rev. Mater. 4, 034409 (2020).
- [26] S. N. Guin, P. Vir, Y. Zhang, N. Kumar, S. J. Watzman, C. Fu, E. Liu, K. Manna, W. Schnelle, J. Gooth, C. Shekhar, Y. Sun, and C. Felser, Adv. Mater. 31, 1806622 (2019).
- [27] See Supplemental Material at http://link.aps.org/supplemental/ 10.1103/PhysRevB.103.L020402 for details of first-principles calculation, the calculated results of band structures, and the Berry curvature, and table of parameters obtained experimentally.
- [28] G. Kresse and J. Furthmüller, Phys. Rev. B 54, 11169 (1996).
- [29] J. P. Perdew, K. Burke, and M. Ernzerhof, Phys. Rev. Lett. 77, 3865 (1996).
- [30] P. E. Blöchl, Phys. Rev. B 50, 17953 (1994).
- [31] G. Kresse and D. Joubert, Phys. Rev. B 59, 1758 (1999).

- [32] Y. Yao, L. Kleinman, A. H. MacDonald, J. Sinova, T. Jungwirth, D.-S. Wang, E. Wang, and Q. Niu, Phys. Rev. Lett. 92, 037204 (2004).
- [33] T. Seki, A. Miura, K. Uchida, T. Kubota, and K. Takanashi, Appl. Phys. Exp. 12, 023006 (2019).
- [34] T. Kikkawa, M. Suzuki, R. Ramos, M. H. Aguirre, J. Okabayashi, K. Uchida, I. Lucas, A. Anadón, D. Kikuchi, P. A. Algarabel, L. Morellón, M. R. Ibarra, and E. Saitoh, J. Appl. Phys. 126, 143903 (2019).
- [35] C. Klewe, T. Kuschel, J.-M. Schmalhorst, F. Bertram, O. Kuschel, J. Wollschläger, J. Strempfer, M. Meinert, and G. Reiss, Phys. Rev. B 93, 214440 (2016).
- [36] N. F. Mott and H. Jones, in *The Theory of the Properties of Metals and Alloys* (Clarendon, Oxford, 1936), pp. 308–314.
- [37] H. Ohta, S. Kim, Y. Mune, T. Mizoguchi, K. Nomura, S. Ohta, T. Nomura, Y. Nakanishi, Y. Ikuhara, M. Hirano, H. Hosono, and K. Koumoto, Nat. Mater. 6, 129 (2007).